**Electronic Supplemental Information**

## Supplemental Information 1: Tracking Algorithm Details

The following four sections (ESI 1.1-1.6) detail the main functions of the tracking algorithm.

### Supplemental Methods 1.1: Cell Segmentation and Particle Identification

For ACT*IV*E cell segmentation and particle identification, time-lapse images are first subjected to a band-pass filter [1]. Based on pixel intensities and a user defined maximum number of contour levels, filtered images are segmented into intensity maps via MATLAB's built-in contour function. The use of contours in nuclear segmentation was pioneered by Idema and colleagues and originally developed to analyze mitotic wavelets in the *Drosophila* embryo [2]. For ACT*IV*E, the Idema approach (originally written in IDL) was translated to MATLAB. For each resultant contour, ACT*IV*E determines a center of mass and maximum. These values are used to establish relationships between contour levels and, ultimately, group series of contours together to identify individual cells. Each cell is processed according to its profile at or above a fit height, where the standard fit height is defined as half height but can be varied by the user for more accurate cell identification. In the case of isolated cells, where every contour above the fit height has only one child contour, the cell is fit according to the Fitzgibbon method [3]. The remaining cells are tagged as possible interactions and are analyzed and categorized as divisions, merging events, or special cases (ESI Methods 1.2–1.5).

### Supplemental Methods 1.2: Defining Interacting Cells

To enable processing of dividing or merging cells and other special cases that may arise, we took advantage of the potential for the contour data to be used to distinguish intensity variations that otherwise appear as a single entity when a threshold is applied. When two nuclei are in close proximity, an interaction event is established and attributed to a cell division or merging event based on prior contour and cell history (ESI Figure S1.1A). In either case, the nuclei involved in the division or merging event share at least one parent contour (ESI Figure S1.1B). These instances are first analyzed at a user chosen fit height contour level, with an ellipse matched accordingly. The default fit height is half height in the current work. The difference in intensities between the two dividing or merging cells results in multiple contour peaks. Correspondingly, an ellipse is fit to each peak for proper cell identification. To ensure that these peaks are not resulting from local noise fluctuations, the area of the fit ellipse is assessed. The ellipse area must fall within the specified bounds of the area interval requirements for the intensity cluster to be fit as two separate ellipses at the first individual contour level (ESI Figure S1.1 C). The contours are otherwise labeled as a multi-peak "special case," which may result either from intensity fluctuations within regions of a nucleus or from background noise that is not signal from a stained nucleus. For these "special cases", the highest shared contour is first identified and fit as a representative ellipse for that particular case. In order to be identified as a cell and included for further tracking analysis, the area criteria for the fit ellipse must be met. Otherwise the intensity fluctuations are attributed to background noise in the system and the contours are removed from the tracking analysis. Currently, ACT*IV*E identifies cells that participate in complex merging events that involve more than two cells, but ACT*IV*E does not incorporate post-processing (i.e., linking corrections) of these more complex events (three or more cells) at this time.

**Supplemental Methods 1.3: Particle Tracking**

Following the contour-based segmentation achieved with the ACT*IV*E approach, the previously established Kilfoil linking method is then utilized to connect cells between consecutive images [1]. In the approach adapted from Kilfoil, the number of identified particles is first recorded for each image. Successive images are then compared and each cell is separated as a trivial or non-trivial case. Trivial cases exist when only one potential cell match is found frame to frame within a specified area. Non-trivial cases result from multiple potential matches and are sorted by minimizing overall distances between particles in a specific area. After sorting, each particle is granted an individual identification tag (ID), which is then used to perform the merging correction and cell division identification. It is important to note that interaction events identified during the segmentation phase are not dealt with during the linking process. Initial IDs are assigned during linking and are later updated during the post-processing step based on their merging or division classification.

**Supplemental Methods 1.4: Merging Correction**

If cells come into close contact, a two-frame positional analysis of the type described in Section 1.3 is often inadequate for capturing and correctly identifying cell IDs. Therefore, to correct for mislabeled IDs following completion of the particle tracking step of ACT*IV*E, cell interactions are first sorted and classified as division or merging events based on their cell ID history. Division events are identified when only one of the two interacting cells has prior track history (ESI Video V1.1). In contrast, when both cells have an ID history prior to the interaction time-point, the event is considered a merging event (ESI Video V1.2). For cells flagged as merging events, a complete profile of the event history is developed for correction analysis. The user specifies a maximum interaction interval (number of frames), which is used to determine the maximum number of frames one cell can completely occlude a second cell and still be considered part of the same merging event. Instances of interaction pairings between the same two cells within that time interval are then established and processed by the ACT*IV*E cost function.

Accurate identification of merging events relies on the ACT*IV*E cost function approach, which incorporates a multi-frame positional or two-frame fingerprint analysis, depending on characteristics of the merging event. A position cost function is employed for every pair of frames where both cell IDs are present in the merging profile. The general equation for positional analysis is defined as:

$$cost = \sqrt{(x_1 - x_2)^2 + (y_1 - y_2)^2} \qquad (S1)$$

where $(x_1, y_1)$ and $(x_2, y_2)$ represent the center of masses for a cell in frames 1 and 2 respectively. All possible combinations for the two IDs are tested, and the minimum cost combination is then selected as the correct IDs for that particular case. However, in cases where a single cell is occluded for multiple consecutive frames, a positional analysis of this type can result in reduced accuracy, due to the time gap in a single cell's tracked data. Therefore, if a single cell is occluded for more than a predetermined number of consecutive frames (chosen as >3 frames in the present work), an alternative cost function is employed, utilizing the area, average intensity, and integrated intensity in a separate "fingerprint" analysis to correct cell IDs. The general equation for the fingerprint analysis is defined as:

$$FP\ cost = w_{II} * \left(\frac{II_1}{\overline{II_1}} - \frac{II_2}{\overline{II_2}}\right)^2 + w_{NI} * \left(\frac{NI_1}{\overline{NI_1}} - \frac{NI_2}{\overline{NI_2}}\right)^2 + w_A * \left(\frac{A_1}{\overline{A_1}} - \frac{A_2}{\overline{A_2}}\right)^2 + w_{AR} * \left(\frac{AR_1}{\overline{AR_1}} - \frac{AR_2}{\overline{AR_2}}\right)^2 + w_P * \left(\frac{\left[\sqrt{(x_1 - x_2)^2 + (y_1 - y_2)^2}\right]}{\left[\frac{\overline{d_1} + \overline{d_2}}{2}\right]}\right)^2 \qquad (S2)$$

where *II* represents the integrated intensity value for a cell, *NI* is the normalized intensity value for a cell, *A* is the area of a cell, *AR* is the aspect ratio of a cell, *d* is the diameter for a cell, *w* represents a weight value for the subscripted variables previously defined (*P* = position in this case, as related to the positional cost function in Eq. *S*1 above) and numerical subscripts denote frame numbers. For our analysis, $w_{II}$, $w_{NI}$, $w_A$, and $w_{AR}$ were set to 1 and $w_P$ was set to 0.

Again, costs for all possible combinations for the two cells are tested, and the minimum cost combination is then selected as the correct IDs for that particular case. In both the position and fingerprint cost case, the lowest resulting normalized cost is identified as the correct ID combination. In instances where the ID combination from either the frame-by-frame positional breakdown or fingerprint method was initially correct, no further steps are taken. However, if the combination is incorrect, the corresponding cell IDs are added to an ID map for subsequent updating. After all events have been assessed, the cell IDs are updated backwards from the end of the tracking analysis to ensure consistency of labeling and proper overall identification.

**Supplemental Methods 1.5: Division Correction**

Following identification of cell divisions it is necessary to post-process these tagged events and eliminate erroneous divisions due to boundary conditions and initial cell interactions, as well as duplicate the parent information so both daughter cells contain complete tracks. To remove false divisions attributed to boundary conditions, or cell interactions that occur as new cells enter the frame, a border width parameter is specified. Any cell interaction occurring within this width is reclassified as an incorrect division and removed from further division analysis. To remove false divisions attributed to cell interactions at the beginning of an image stack, a user may reclassify any divisions that occur within a preset number of frames of the start of the stack, as these early events may account for a large number of false divisions, especially at large densities, because many cells will be experiencing merging interactions at the onset of imaging, which can lead to erroneous classification as divisions. Also the area of the two daughter cells are compared; if the area difference is larger than a user-specified threshold the division is no longer classified as a division, further reducing the number of false positive division identifications. Following correction of misclassified divisions, the parent information of each division is duplicated and assigned to the new daughter cell. This ensures each daughter cell has complete tracks prior to the division event, rather than randomly assigning one of the two daughter cells the parent cell's prior track information.

**Supplemental Methods 1.6: User Defined Input Parameters**

ACT*IV*E requires a set of user-defined input parameters to be specified prior to tracking. These parameters are summarized in Supplement Table T1.1, with the values used in this study shown. A set of plotting toggles are also required (plottoggle and collision_plot_toggle) which allow the user to generate images of the segmentation (contours and fit-ellipses) and post-processing of cell merging events (before and after post-processing), respectively. A set of hardcoded parameters also exist which allow the user to optimize the segmentation and post-processing for a given application: fit_height, which determines the contour level to which an ellipse is fit; maxdup, which controls how long a cells can completely occlude before a fingerprinting method is used for linking; and a series of weighting parameters for fingerprint analysis. For more information about these parameters please refer to the user manual available with download of ACT*IV*E (see main text for download instructions).

**Supplement Table T1.1.** User defined input parameters, including values used in this study, a brief description of the parameters, and the tracking step that employs each parameter..

| Parameter | Value | Brief Description | Tracking Step |
|---|---|---|---|
| nlevels | 15 | # of contour levels for intensity map | segmentation |
| halfobjectsize | 13 | radius of particles, pixels | segmentation |
| noise_wavelength | 2 | lengthscale of noise, pixels | segmentation |
| area_thresh | 260 | maximum cell area, pixels$^2$ | segmentation |
| min_area | 10 | minimum cell area, pixels$^2$ | segmentation |
| maxdisp* | 20 (17) | maximum distance migrated between 2 consecutive frames, pixels | linking |
| max_collision_time | 10 | # of frames a complete occlusion can occur | linking |
| frametime | 3 | time between frames | post processing |

*For maxdisp, a value of 20 was used for cell seeding densities of 5,000 and 10,000 cells/cm$^2$, whereas a value of 17 was used for cell seeding densities of 20,000 cellscm$^2$

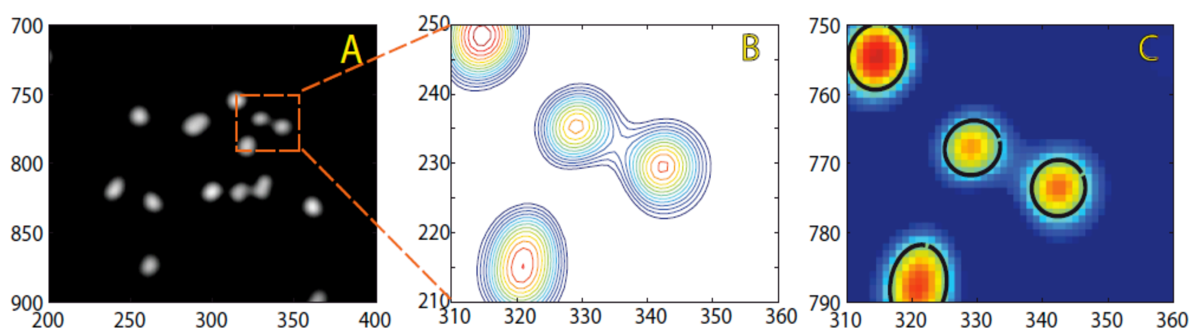


**Supplement Figure S1.1: Interacting cells are detected as cells sharing a common contour.** A) After applying the bandpass filter to remove noise from local intensity variations, contour profiles are generated from the intensity maps. B) Interacting cells share at least one parent contour (lower level contours). Higher-level contours above the last shared contour are used to identify each individual cell, and C) an ellipse is fit to the half-height contour (black).

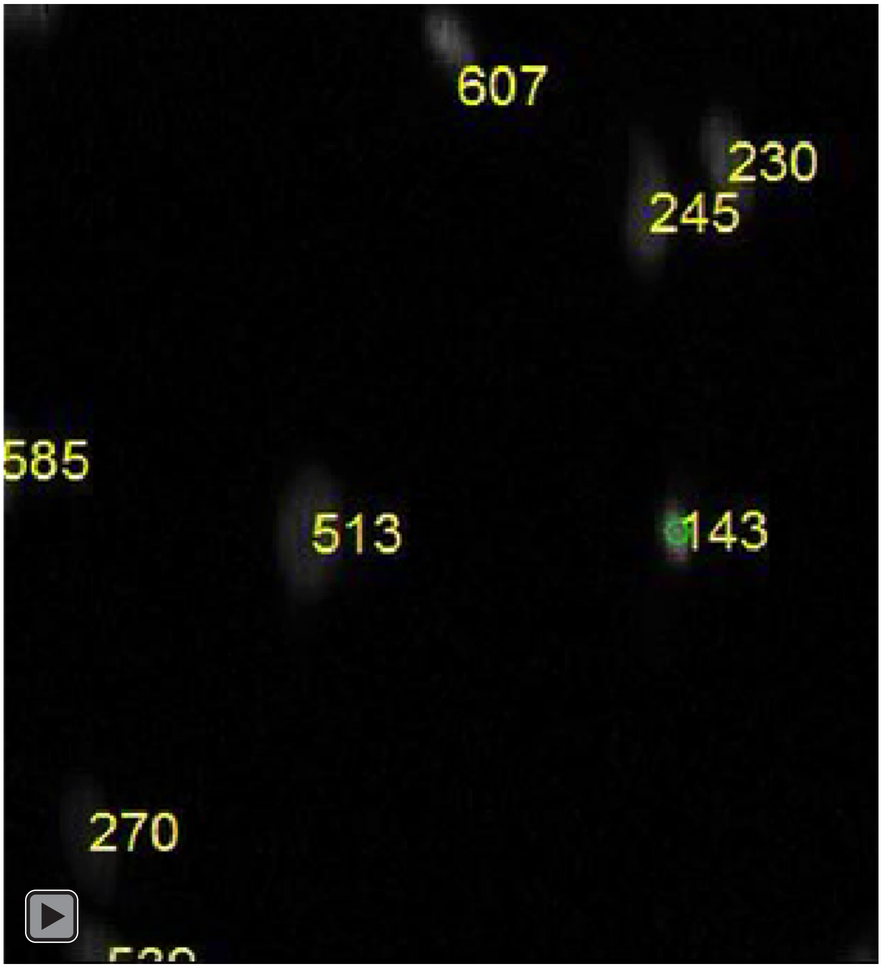


**Supplement Video V1.1: Cell division events are identified, tagged and tracked.** Frames prior to a cell division indicate the condensing of the cell nucleus, followed by successful division of the cell. Frames following the division event show that the two cells are individually segmented and given IDs, but remain flagged as sibling cells**.**

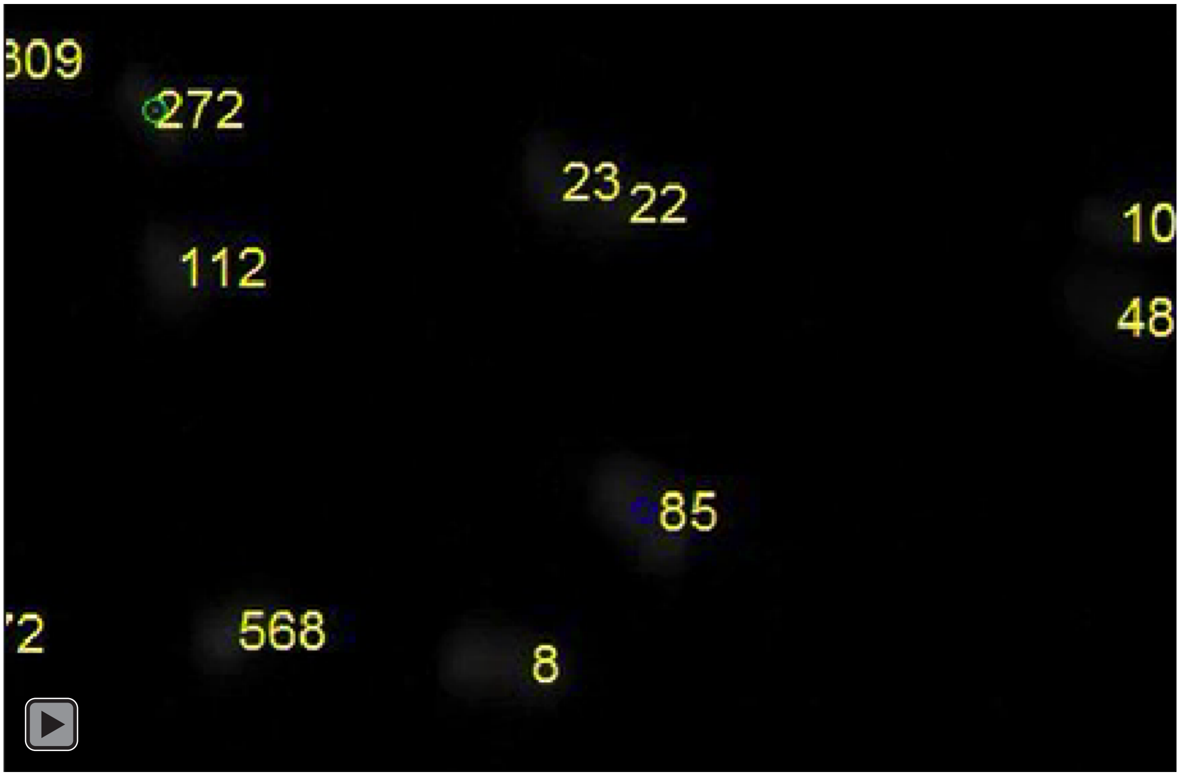


**Supplement Video V1.2: A customized cost function is used to analyze and correct cell IDs involved in merging events.** Two cells come in close contact causing an occlusion event to occur. During occlusion, one cell ID is lost. To ensure proper re-identification, our customized fingerprint function is employed to properly sort cell IDs.

**Supplemental Information 2: Segmentation Validation and Benchmarking Analysis**

The following sections detail the validation of the ACT*IV*E contour-based segmentation approach using synthetic data.

**Supplemental Methods 2.1: Synthetic Data Generation**

Synthetic data was generated using an active matter simulation with periodic boundary conditions as discussed in previous work [4]. Briefly, two datasets were generated for active matter particles at two different densities. The densities, quantified as the percentage of total image area occupied by cell nuclei, were 11.1 % and 17.1 %, respectively. These datasets simulate cell experiments of the type employed in the experimental application of ACT*IV*E (ESI Methods 3.1-3.2), but without cell division and without cell-cell occlusion. The active matter particles were simulated for 4000 natural simulation time units, with overdamped dynamics using the equations as described in work by Henkes and colleagues [4], with one alteration; the drag coefficient in the y-direction was four times as high as the drag coefficient in the x-direction to mimic the anisotropy in the experimental data. Model parameters were: a spring constant (K) of 1, a drag coefficient (b) in the x-direction of magnitude 1, a self-propelled velocity (v0) of magnitude 0.1, and a rotational noise ($\eta$) of magnitude 0.1 in simulation units. Synthetic images are generated on a black background by placing a randomly oriented white ellipse with eccentricity 2 centered at each active particle position. Detailed x, y, and z positional and time frame data was recorded for each set for comparison to ACT*IV*E and Kilfoil methods. Synthetic datasets were run through ACT*IV*E and the Kilfoil methods and the resulting positional data was compared to the known synthetic tracks for an accuracy comparison. Because the synthetic data did not include divisions or occlusions, the comparison between ACT*IV*E and the Kilfoil benchmark is most useful in validating the accuracy of the ACT*IV*E contour-based segmentation (vs. the Kilfoil local high intensity segmentation approach).

**Supplemental Methods 2.2: Synthetic Accuracy Determination**

To determine the accuracy of cell tracks over time for the ACT*IV*E and Kilfoil (benchmark) approaches, cells were first segmented for the first frame by each automated approach. These segmented cells were then mapped to the synthetic data based upon location, with each segmented cell ID being assigned a corresponding synthetic cell ID. For each of the following 479 frames, this cell ID map was used to determine if the cell IDs assigned from the ACT*IV*E and Kilfoil approaches matched the corresponding IDs in the synthetic data. Track accuracy was calculated as the percentage of these cells that were assigned the correct cell IDs. An accuracy value was attained for each frame and plotted as a function of time (ESI Figure S2.1). This procedure was also used to calculate an accuracy for the previously established automated method. Track inaccuracies could result from cells not being segmented, and thus the cell ID being absent, or cell IDs being assigned to the wrong cells. Fluctuations in the accuracy occur because of the former, where cell IDs may be lost during one frame (due to segmentation limitations) but reappear and be correctly ID'd in a subsequent frame. This under-segmentation arises from smoothing the intensity profile using a bandpass filter, where cells that are partially occluded will have smeared and overlapping intensity profiles with no distinction in the contour profile. This may be improved through increasing the number of contours, but at the cost of increased computation time.

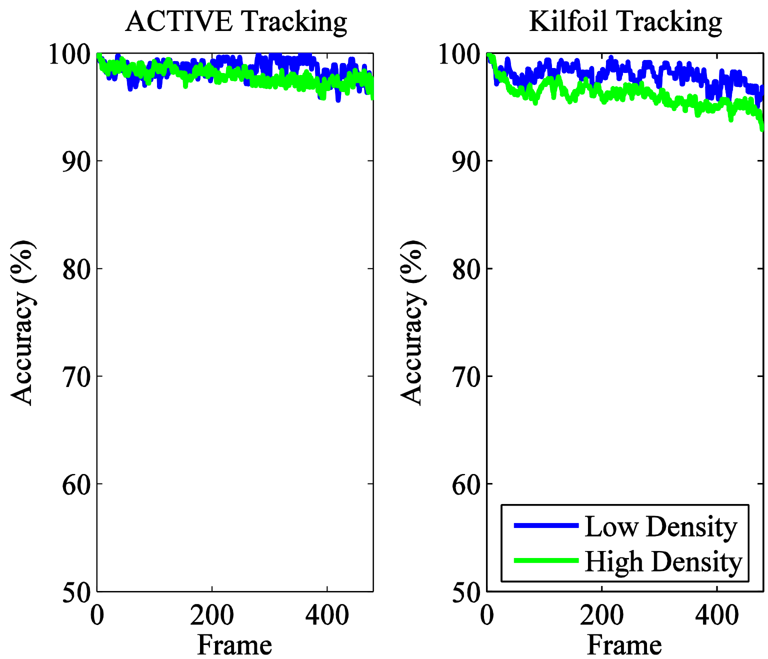


**Supplement Figure S2.1: Tracking accuracy of ACTIVE and Kilfoil approaches.** Accuracy of ACT*IV*E (left) and Kilfoil (right) at both high (green) and low (blue) simulated cell seeding densities reveal that both Kilfoil and ACT*IV*E can track cells at low and high densities with high accuracy. Because cells in the synthetic datasets do not divide nor occlude, the comparison between ACT*IV*E and the Kilfoil benchmark is most useful in validating the accuracy of the ACT*IV*E contour-based segmentation (vs. the Kilfoil threshold-based segmentation).

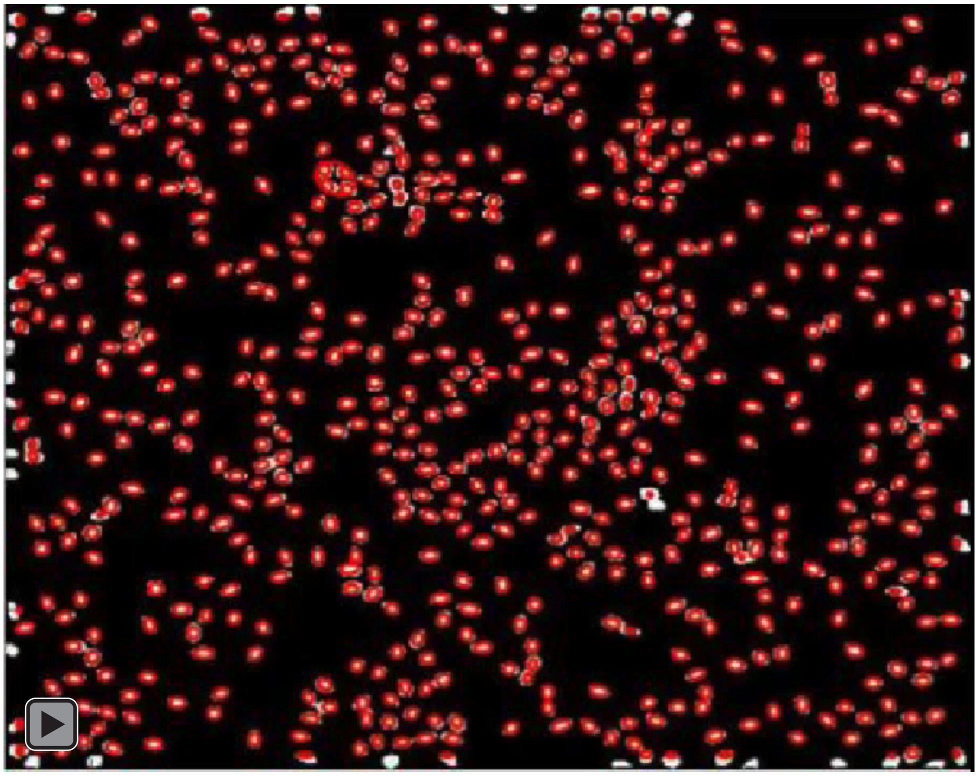

**Supplement Video V2.1: Synthetic data generated at a representative high cell density for ACT*IV*E and Kilfoil segmentation accuracy comparison.** Red ellipses denote fits generated by the ACT*IV*E system for synthetic cell tracking.

**Supplemental Information 3: Cell Experiments**

The following sections detail the cell culture experiments used both to benchmark ACT*IV*E and to provide new insights into cell behavior in anisotropic environments.

**Supplemental Methods 3.1: Cell Culture**

For cell experiments, C3H10T1/2 mouse fibroblasts (ATCC) were first expanded in complete growth medium (BME, 10 % FBS, 1 % penicillin/streptomycin, 1 % GlutaMAX) on T75 flasks, with initial seeding at 5,000 cells/cm$^2$. Expansion was conducted in a humidified incubator with 5 % $CO_2$ at 37 °C. Medium was changed after 3 d, and cells were passaged at 80 % confluence using 0.25 % Trypsin. Cells at passage 13-15 were used for experiments. Samples were prepared for cell tracking experiments by seeding cells on wrinkled, non-wrinkled, and TCPS substrates. To study the effects of varying density, cells were seeded onto 6 mm × 6 mm substrates using a droplet method at 5,000, 10,000 or 20,000 cells/cm$^2$. In each case, a 20 µL droplet of cell solution was seeded onto the substrates with cell concentrations of 87,500, 175,000, and 350,000 cells mL$^{-1}$, respectively, and samples were then placed in a 37 °C incubator for 2 h to allow for cell attachment. After 2 h, complete growth medium was added and the samples were placed in a 37 °C incubator for an additional 22 h, at which point the cells were stained and prepared for live cell imaging. The resulting experimental densities demonstrated nuclear area densities, quantified as the percentage of total image area occupied by cell nuclei, of approximately 3.12%, 5.23%, and 6.36%, respectively, as measured in representative images. These experimental densities were, therefore, lower than the range of densities used for the synthetic data during validation (11.1 % and 17.1 %).

**Supplemental Methods 3.2: Cell Staining and Imaging**

To image cell nuclei for tracking analysis, cells were stained with Hoechst 33342 nuclear dye and imaged over 24 h. Hoechst dye was added to complete growth medium at a concentration of 0.01 μg $mL^{-1}$. A concentration significantly lower than the recommended staining concentration was deliberately selected both to test the ability of ACT*IV*E to segment cells of low contrast and to ensure cell divisions throughout the 24 h time period (as Hoechst dye at the recommended concentration significantly suppressed cell division – data not shown). Using a low staining concentration also enabled live cell imaging over a longer period of time due to reduced phototoxicity when compared to higher concentrations tested in preliminary studies. Substrates with attached cells were placed in LabTek glass-bottom chamber slides and 800 µL of staining solution was added to each chamber. The chamber slide was then placed in a 37 °C incubator for 20 min to allow for cell nuclei to be stained. Substrates were then inverted in the chamber slide and a hemocytometer glass coverslip was placed on top of each sample for stabilization. The glass chamber slide was placed in a live cell incubator (INC-2000, 20-20 Technology Inc.) and imaged on a Leica DMI 6000B inverted microscope. Live cell imaging was conducted at 37 °C for 24 h under 5 % $CO_2$, with images captured every 3 min using an Andor Luca R camera with a 10x/0.30 NA objective.

**Supplemental Information 4: Benchmarking of Execution Time and Accuracy (Event and Division Detection)**

The following sections detail the method for determining execution time and accuracy during comparison of manual tracking, ACT*IV*E, and the Kilfoil approach [1].

**Supplemental Methods 4.1: Determination of Execution Time**

To determine execution time, cropped image substacks were generated from experimentally acquired stacks of cells seeded at 10,000 cells/cm$^2$ (the middle of the three cell densities studied) on wrinkled or TCPS substrates to reflect anisotropic and isotropic substrates, respectively. For the isotropic group, a TCPS substack was chosen instead of a flat, gold-coated substrate to investigate manual tracking of low-contrast images, because the TCPS images showed the lowest contrast of all groups and therefore the most rigorous validation of ACT*IV*E. Each substack consisted of 30-50 cells and was 50 frames in length. Manual tracking with MTrackJ [5], an ImageJ plugin, was performed. The same trained user performed all manual tracking.

**Supplemental Methods 4.2: Determination of Event Accuracy**

Assessment of automated tracking accuracy focused on the extent to which the two automated approaches could accurately track non-trivial cell cases. Trivial cases were defined as any cases where only one potential cell match is found frame-to-frame within a specified area. The focus on non-trivial cases was chosen because both ACT*IV*E and the Kilfoil tracking approach were observed to track trivial cases with accuracy at or near 100 %. The ability of the automated approaches to accurately track non-trivial cell cases was determined by first generating 100 videos of merging events, as identified from ACT*IV*E. The identified merging events included cases of frame-by-frame positional and fingerprint analysis by ACT*IV*E to ensure accuracy of both methods. Next, an expert user determined whether each event could be manually tracked with confidence. If it could be manually tracked, the expert user then determined if the two automated approaches had correctly tracked the cells involved in the merging event. The resulting measure of accuracy was determined as the number of events that were correctly labeled divided by the total number of events that could be manually tracked with confidence.

**Supplemental Methods 4.3: Determination of Division Detection Accuracy**

False positives, or events inaccurately labeled as divisions, were determined by isolating 100 of the 323 events labeled as divisions from the same wrinkled stack used for the benchmarking analysis. A video of each division event was generated and manually analyzed to determine if the event was a true division or a false positive. False negatives, or divisions that were not identified by the ACT*IV*E approach, were determined by overlaying each identified division on the original image stack. An expert viewer then manually stepped through the overlaid stack and identified cell divisions that were not identified by the ACT*IV*E approach.

**Supplemental Information 5: Cell Motility Results Comparison**

The following sections detail cell motility analyses performed for cells seeded on different substrates and at various densities.

**Supplement Table T5.1.** Average number of cells identified by ACT*IV*E for various frames at each density and substrate type.

| Density (cells/cm$^2$) | Material Type | Average Number of Cells Segmented in First Frame | Average Number of Cells Segmented in Last Frame | Average Total Number of Cells Identified by ACT*IV*E Over All Frames |
|---|---|---|---|---|
| 5,000 | Wrinkled | 327 ± 118 | 344 ± 171 | 760 ± 347 |
| | Non-Wrinkled | 278 ± 61 | 308 ± 56 | 716 ± 112 |
| | TCPS | 405 ± 260 | 348 ± 213 | 956 ± 650 |
| 10,000 | Wrinkled | 611 ± 145 | 597 ± 152 | 1196 ± 465 |
| | Non-Wrinkled | 662 ± 130 | 590 ± 88 | 1519 ± 480 |
| | TCPS | 725 ± 239 | 636 ± 217 | 1558 ± 586 |
| 20,000 | Wrinkled | 898 ± 389 | 746 ± 234 | 1627 ± 729 |
| | Non-Wrinkled | 869 ± 316 | 652 ± 150 | 1943 ± 1164 |
| | TCPS | 1097 ± 347 | 780 ± 137 | 2670 ± 989 |

**Supplement Table T5.2: MSD parameters for substrates.** Average slopes and mobility parameters are reported for the non-decomposed and decomposed MSD profiles. Standard deviations are in parentheses. For substrates, wrinkled = W, non-wrinkled = NW, and tissue culture polystyrene = TCPS. For a given metric (column), statistical comparisons were made between substrate type (W vs. NW vs. TCPS). For each metric, substrates sharing a label are statistically different. Substrates that do not share a label are not statistically different.

| | | Non-decomposed MSD | | | Decomposed MSD | | | | | |
|---|---|---|---|---|---|---|---|---|---|---|
| | | Short Timescale Slope | Long Timescale Slope | δ | X-Short Timescale Slope | X-Long Timescale Slope | X- δ | Y-Short Timescale Slope | Y-Long Timescale Slope | Y- δ |
| Substrate | W | $1.67^{a}$ (0.09) | $1.32^{a}$ (0.13) | 0.45 (0.52) | $1.71^{a,b}$ (0.09) | 1.33 (0.13) | 0.37 (0.54) | 1.52 (0.11) | 1.23 (0.09) | -0.25 (0.42) |
| | NW | $1.53^{a}$ (0.13) | $1.32^{b}$ (0.11) | 0.18 (0.51) | $1.53^{a}$ (0.12) | $1.34^{a}$ (0.12) | -0.16 (0.55) | 1.53 (0.14) | 1.28 (0.12) | -0.07 (0.48) |
| | TCPS | 1.56 (0.16) | $1.21^{a,b}$ (0.12) | 0.58 (0.59) | $1.56^{b}$ (0.16) | $1.21^{a}$ (0.15) | 0.27 (0.60) | 1.56 (0.16) | 1.20 (0.12) | 0.31 (0.65) |

**Supplement Table T5.3: Velocity auto-correlation and track asphericity for substrates.** Average track asphericity and the decay constants fit to the velocity autocorrelation function, where x is the direction parallel to the wrinkles for the wrinkled substrate, are reported. Standard deviations are in parentheses. For a given metric (column), statistical comparisons were made between substrate type (W vs. NW vs. TCPS). For each metric, substrates sharing a label are statistically different. Substrates that do not share a label are not statistically different.

| | | Velocity Auto-correlation | | Asphericity |
|---|---|---|---|---|
| | | X-Time Constant x $10^{-3}$ ($s^{-1}$) | Y-Time Constant x $10^{-3}$ ($s^{-1}$) | Track Asphericity |
| Substrate | Wrinkle | -4.85 $(1.29)^{a}$ | -9.99 $(3.24)^{a,b}$ | 0.85 $(0.02)^{a,b}$ |
| | Non-Wrinkle | -5.79 $(1.31)^{b}$ | -6.49 $(1.94)^{a}$ | 0.81 $(0.02)^{a,c}$ |
| | TCPS | -8.35 $(2.04)^{a,b}$ | -7.88 $(2.35)^{b}$ | 0.77 $(0.02)^{b,c}$ |

**Supplement Table T5.4: Average cell density correlation with MSD parameters for different substrates.** Spearman rank correlation coefficients are reported for the average slopes and mobility parameters for the non-decomposed and decomposed MSD profiles. For substrates, wrinkled = W, non-wrinkled = NW, and tissue culture polystyrene = TCPS. Significant correlations are highlighted in yellow.

| | | Non-decomposed MSD | | | Decomposed MSD | | | | | |
|---|---|---|---|---|---|---|---|---|---|---|
| | | Short Timescale Slope | Long Timescale Slope | δ | X-Short Timescale Slope | X-Long Timescale Slope | X- δ | Y-Short Timescale Slope | Y-Long Timescale Slope | Y- δ |
| Substrate | W | -0.189 | -0.053 | -0.329 | -0.063 | -0.021 | -0.305 | -0.809 | 0.046 | -0.469 |
| | NW | -0.551 | 0.053 | -0.503 | -0.601 | 0.261 | -0.434 | -0.539 | -0.459 | -0.357 |
| | TCPS | -0.592 | 0.067 | -0.413 | -0.599 | -0.060 | -0.238 | -0.697 | 0.319 | -0.629 |

**Supplement Table T5.5: Average cell density correlation with velocity auto-correlation parameters and cell track asphericity for different substrates.** Spearman rank correlation coefficients are reported for the decay constants of the velocity auto-correlation fit and for the cell track asphericity. For substrates, wrinkled = W, non-wrinkled = NW, and tissue culture polystyrene = TCPS. Significant correlations are highlighted in yellow.

| | | Velocity Auto-correlation | | Asphericity |
|---|---|---|---|---|
| | | X-Time Constant | Y-Time Constant | Track Asphericity |
| Substrate | Wrinkle | -0.420 | 0.133 | 0.762 |
| | Non-Wrinkle | 0.301 | 0.266 | 0.259 |
| | TCPS | -0.147 | -0.119 | 0.524 |

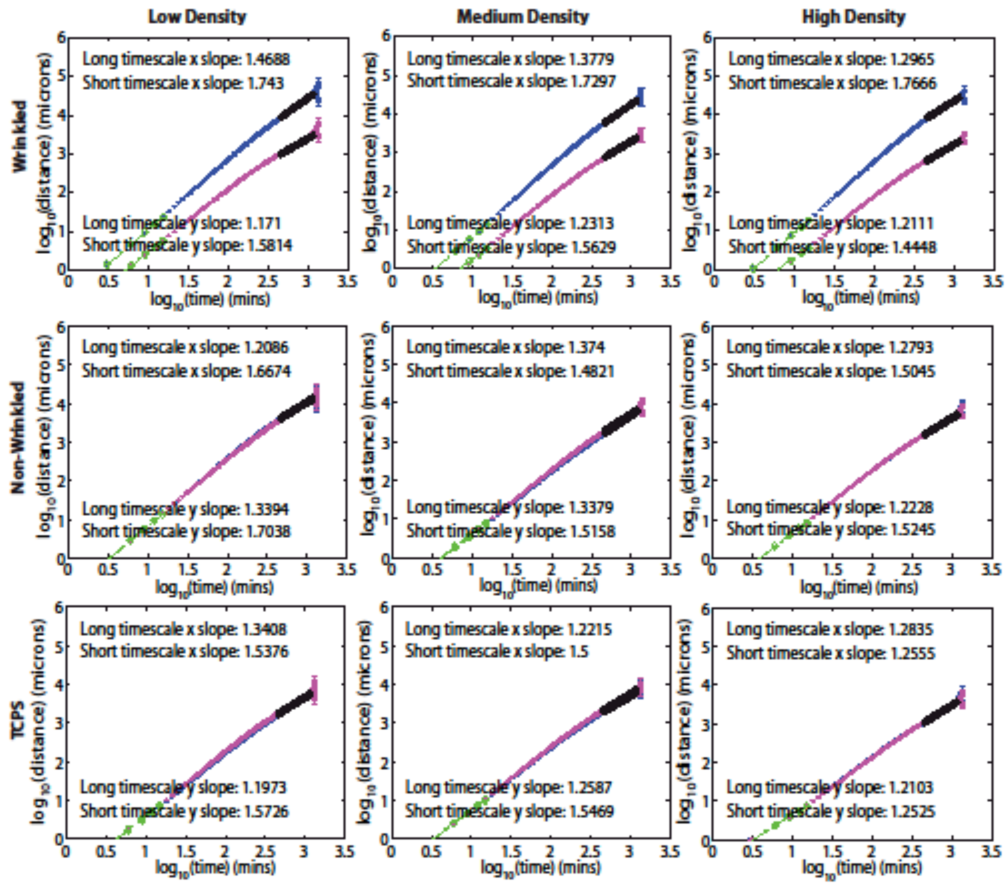


**Supplement Figure S5.1: Representative MSD plots for cells seeded on anisotropic and flat substrates at various densities.** Cells seeded on (top) wrinkled, (middle) non-wrinkled, and (bottom) TCPS at (left) 5,000, (middle) 10,000 and (right) 20,000 cells/cm$^2$ were analyzed using a mean squared displacement correlation analysis. Slopes of the MSD plots were calculated at small timescales and large timescales to determine the diffusive nature of migration. Linear regression was used on the first 5 data points for short timescale slopes and a range of 60 data points for the long timescale slope, using the same range for each sample.

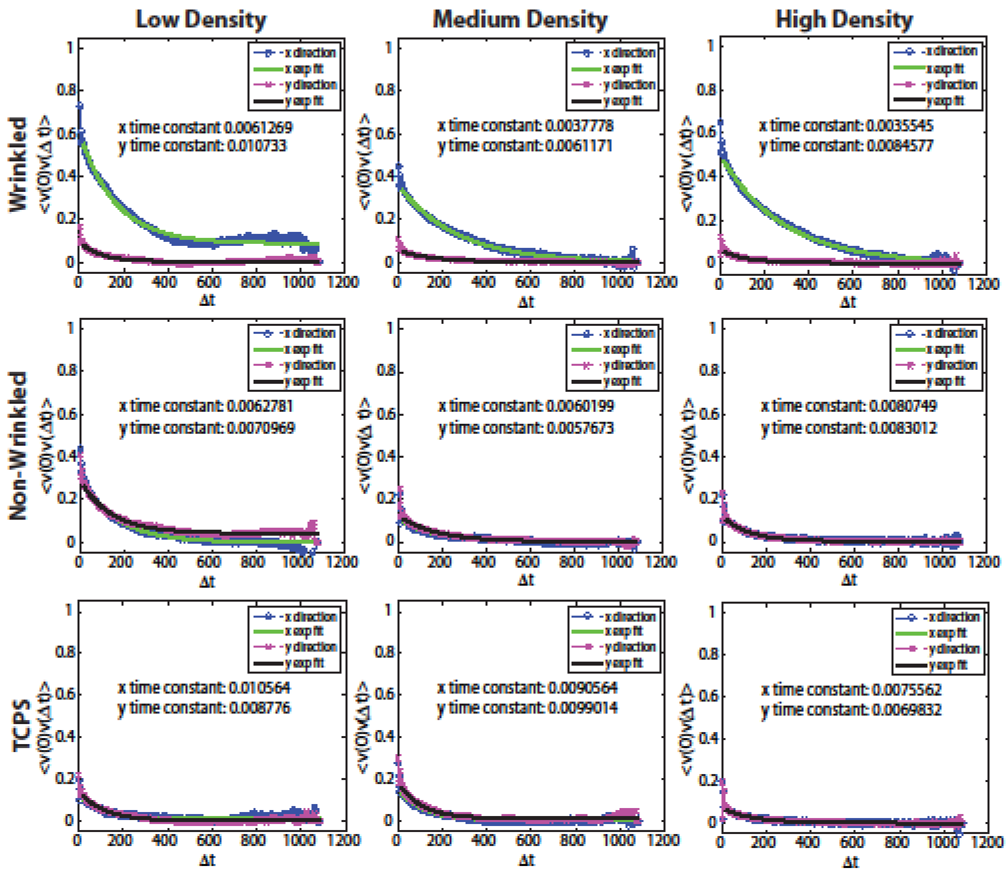


**Supplement Figure S5.2: Representative velocity autocorrelation plots for cells seeded on anisotropic and flat substrates at various densities.** Cells seeded on (top) wrinkled, (middle) non-wrinkled, and (bottom) TCPS at (left) 5,000, (middle) 10,000 and (right) 20,000 cells/cm$^2$ were analyzed using a velocity autocorrelation function. Anisotropic substrates showed distinct preferential migration along the grooved direction, while non-wrinkled and TCPS controls demonstrated no statistically significant difference in their x- and y-velocity autocorrelation components. An exponential decay was fit to each profile after removing the first 5 points due to noise. A decay constant was extracted and compared amongst all samples. In these images x1 refers to the decay amplitude, x2 the decay constant, and x3 the equilibrium offset.

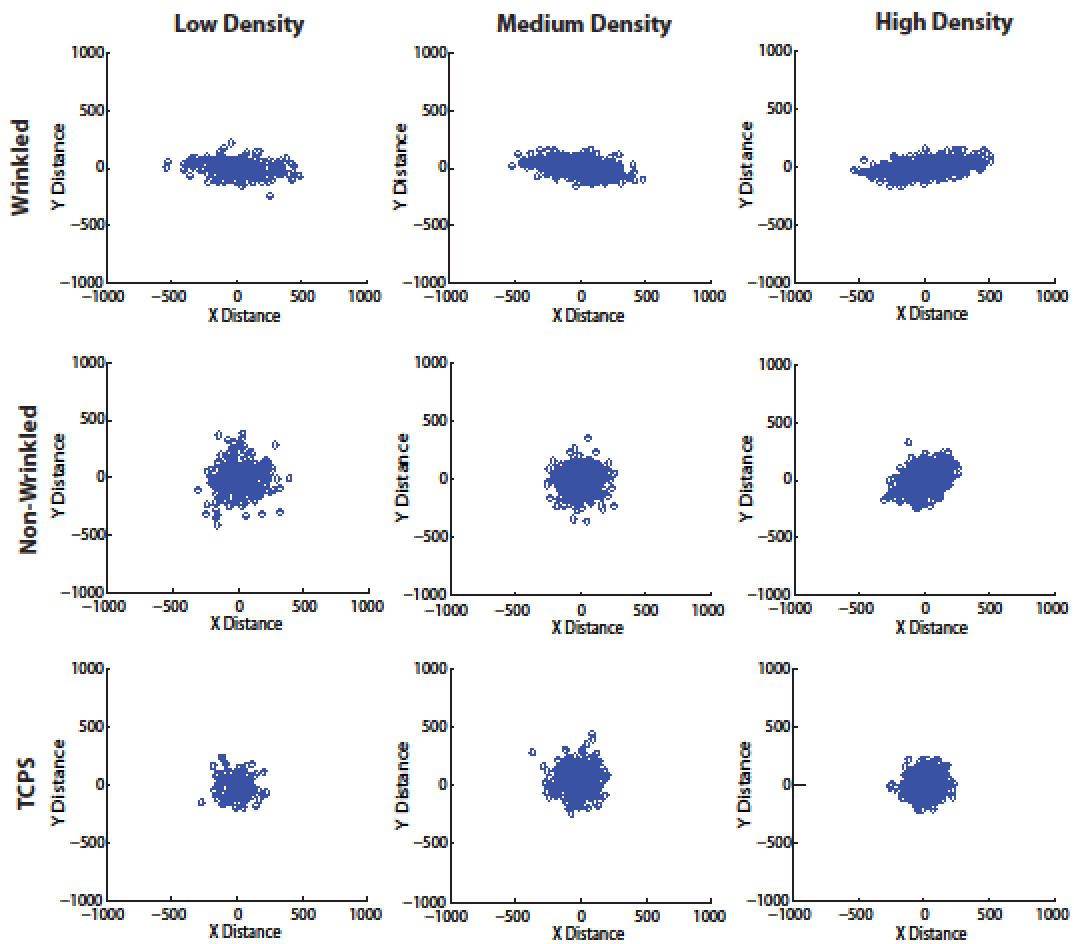


**Supplement Figure S5.3: Representative cell diffusion plots for cells seeded on anisotropic and flat substrates at various densities.** Cells seeded on (top) wrinkled, (middle) non-wrinkled, and (bottom) TCPS at (left) 5,000, (middle) 10,000 and (right) 20,000 cells/cm$^2$ were analyzed when the final position for each cell was plotted after renormalizing the starting location to the plot origin. Anisotropic substrates showed directed cell migration as noted by the location of most cells along the x-axis (parallel to the wrinkle direction). In contrast, cells atop both isotropic substrates showed no preferential migration as noted by the radial distribution of cells from the origin.

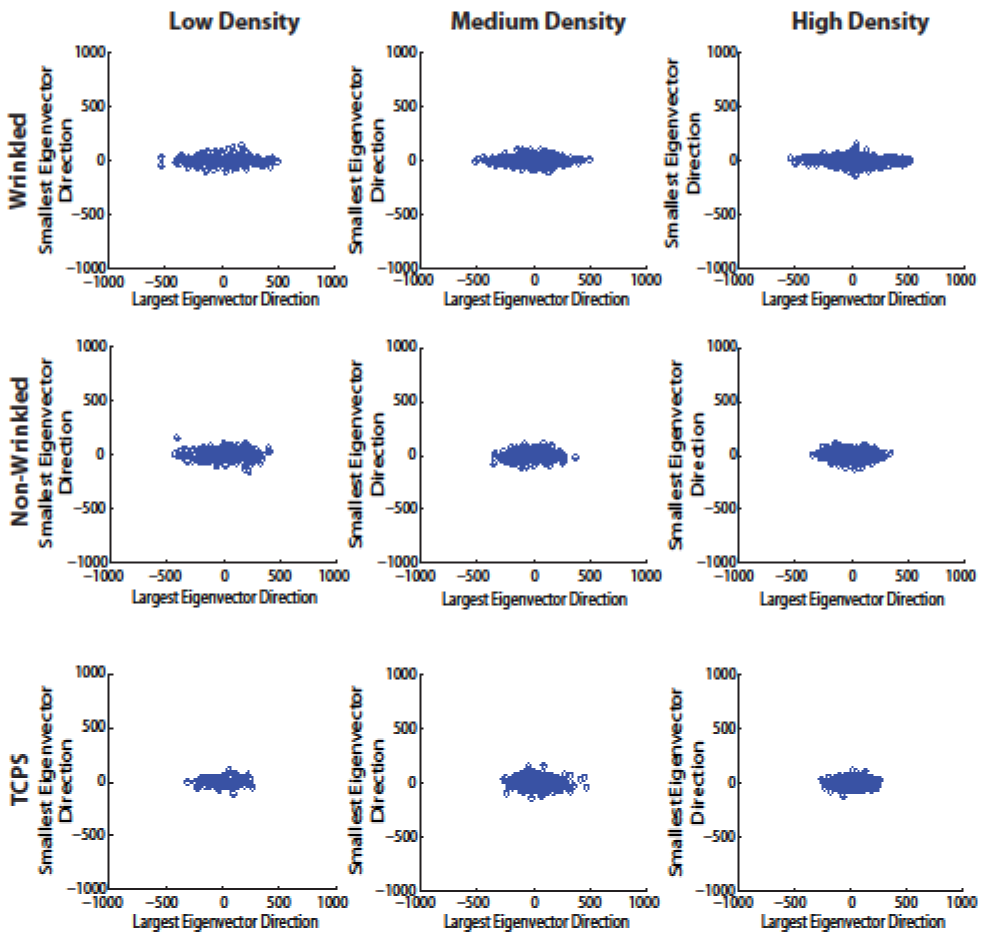


**Supplement Figure S5.4: Representative cell track terminal points for cells seeded on anisotropic and flat substrates at various densities.** Terminal points for cell tracks, for cells seeded on (top) wrinkled, (middle) non-wrinkled, and (bottom) TCPS at (left) 5,000, (middle) 10,000 and (right) 20,000 cells/cm$^2$. Terminal points were rotated so that the largest eigenvector of the gyration tensor (Eq. 3 in the main text) lies along the x-axis. Therefore, the anisotropy of the points is a visualization of average track asphericity. Surprisingly, cell track asphericity was significantly higher atop flat gold substrates when compared to flat TCPS substrates, indicative of a dependence of cell motility on surface chemistry.

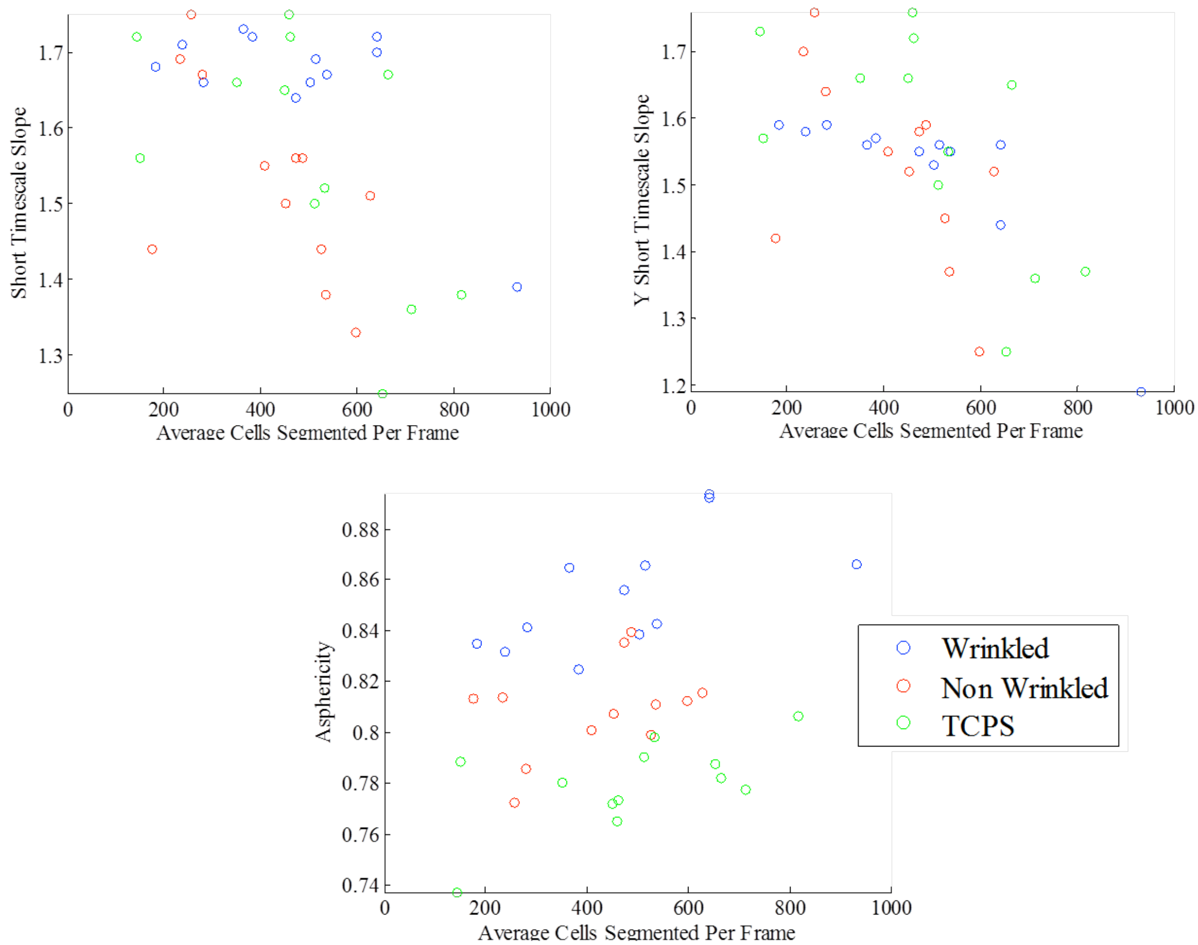


**Supplement Figure S5.5: Cell motility behavior correlation with average cell density.** Short timescale slopes extracted from the non-decomposed and decomposed MSD and cell track asphericity are plotted as a function of the average cell density for a given sample. Short timescale slopes exhibit a negative correlation with cell density, while cell track asphericity is positively correlated with cell density particularly atop the anisotropic wrinkled substrate. Average cell density is determined as the average number of particles segmented in the beginning and ending frames.

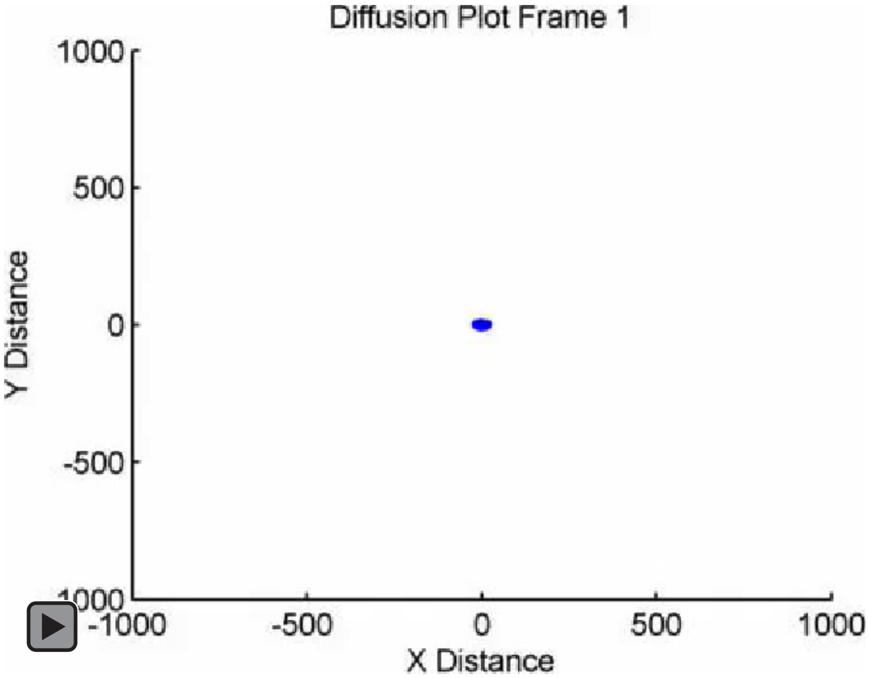


**Supplement Video V5.1: Representative diffusion plot video for wrinkled anisotropic substrate.** Diffusion plots are shown for the lowest experimental density used in the anisotropic vs. isotropic analysis.

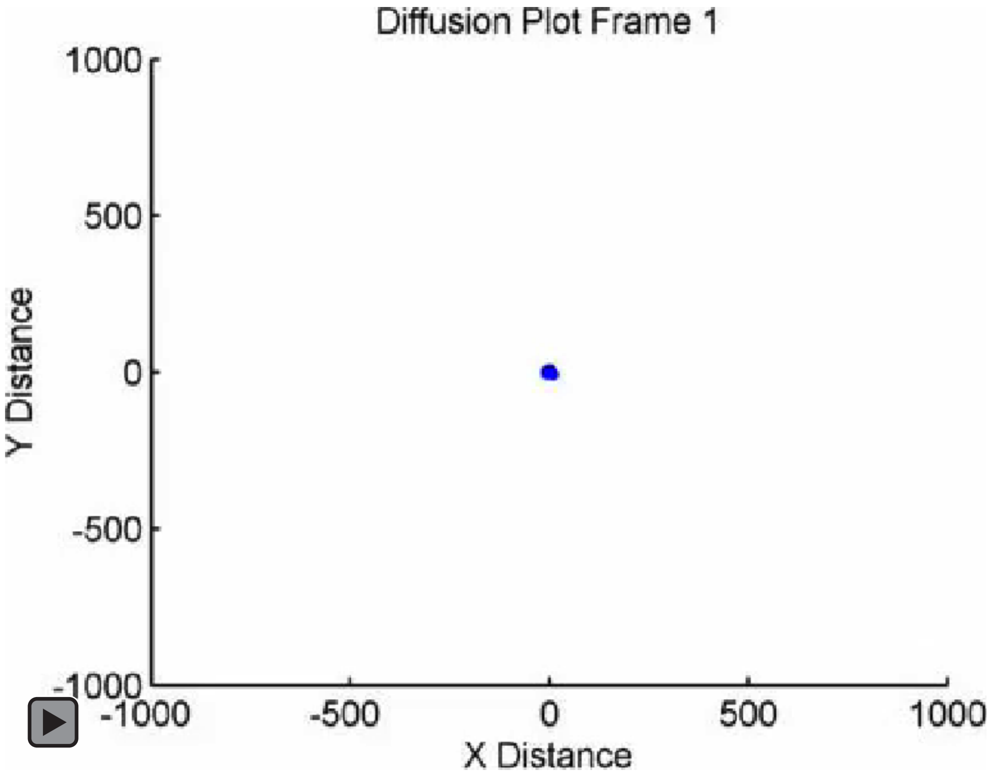


**Supplement Video V5.2: Representative diffusion plot video for non-wrinkled isotropic substrate.** Diffusion plots are shown for the lowest experimental density used in the anisotropic vs. isotropic analysis.

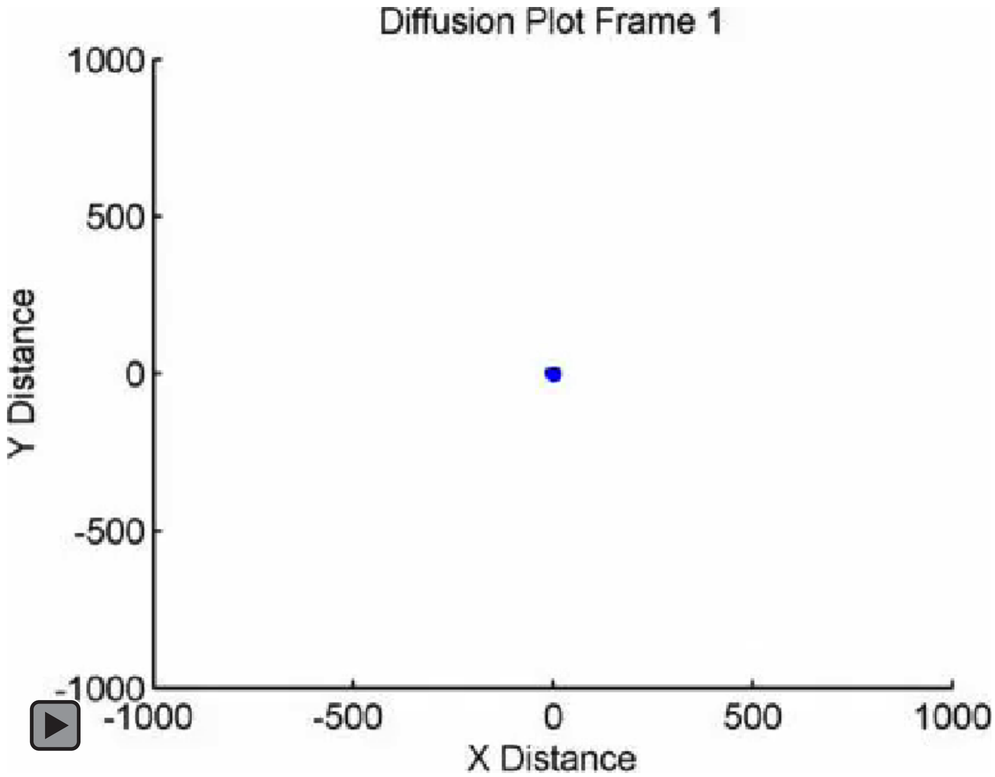


**Supplement Video V5.3: Representative diffusion plot video for TCPS isotropic substrate.** Diffusion plots are shown for the lowest experimental density used in the anisotropic vs. isotropic analysis.

**Supplemental Information 6: Benchmarking**

The following sections detail the results for benchmarking ACT*IV*E with the Kilfoil and manual tracking approaches.

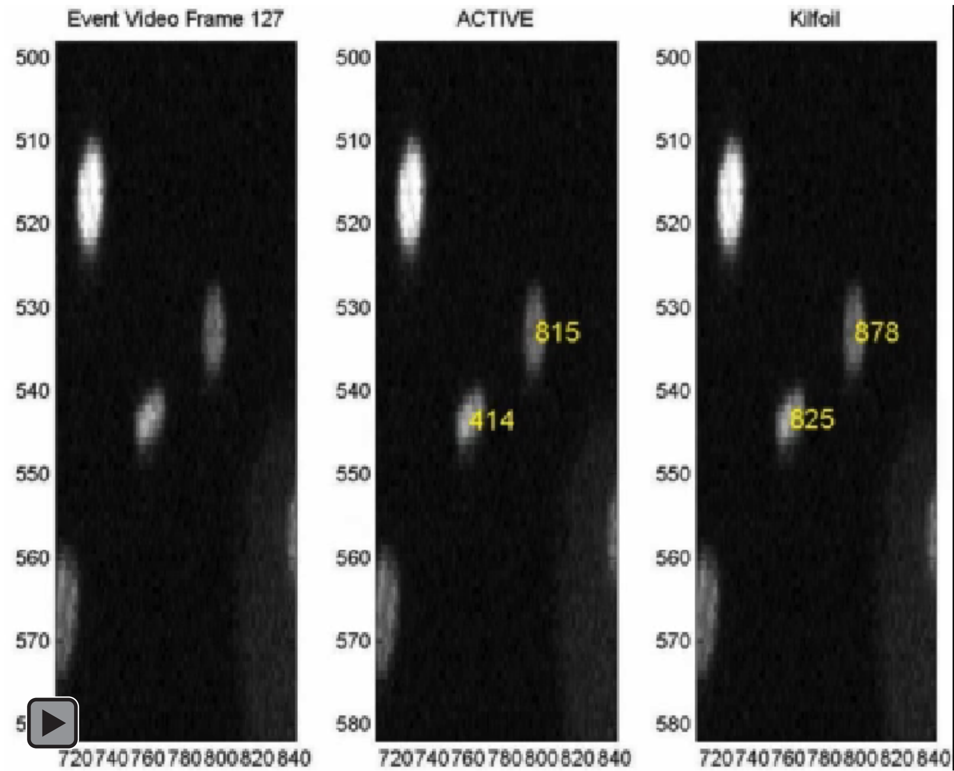


**Supplement Video V6.1: Determining accuracy of the tracking algorithm through investigation of cell merging events.** Videos of (left) the merging event and the two cells involved, (middle) the corresponding ACT*IV*E cell IDs, and (right) the corresponding Kilfoil cell IDs.

**Supplemental Information 7: Division Analysis**

The following section details the division orientation methodology and results used to determine the ability of ACT*IV*E to isolate and analyze cell divisions.

**Supplemental Methods 7.1: Division Directionality and Analysis**

To determine the influence of topography on division directionality—the direction in which the daughter cells pull apart—events flagged as divisions by ACT*IV*E were analyzed. In the first frame the daughter cells pull apart, the angle made between the two centroids and the horizontal axis was calculated. The spread of these division angles was calculated following a protocol used previously to determine angular spread of cell nuclei [6]. Division angles were adjusted so all angles fell in the range of -90° to +90°, centered around 0°. The truncated standard deviation [7] of the divisions was then calculated, yielding the angular spread. To normalize between isotropic and anisotropic substrates, division angles were systematically rotated by 1° from 0° to 180° and the corresponding angular spreads calculated. For each substrate, the reference angle resulting in the minimum angular spread was used. The reference angle yielding the minimum standard deviation was typically within ± 10° of the wrinkle angle for the wrinkled substrates, meaning the division angle occurred parallel to the wrinkles. This is qualitatively shown in Figure S7.1. An angular spread of 52° represents a completely random spread—no preferential division directionality—and a decrease in the angular spread represents an increase in the preferential division directionality.

Statistical analyses were conducted on the angular spread values for each substrate. One factor ANOVA was used to compare all substrates (wrinkled, non-wrinkled, and TCPS) , with an n=12 for each substrate. Individual comparison testing was conducted using a student's t-test, with the Holms-Sidak correction applied to correct for multiple comparisons (3 comparisons). Significance was determined at the 95% confidence level. Results were summarized inTables T7.1-7.2.

**Supplement Table T7.1: Angular spread of division angles atop anisotropic and isotropic substrates.** Average angular spread for the wrinkled substrate is lower than the gold coated and TCPS substrates, indicative of more directed division atop the wrinkled topography.

| | Wrinkled | Non-wrinkled | TCPS |
|---|---|---|---|
| Angular Spread | 41.0 (3.7) | 47.3 (3.1) | 48.5 (2.9) |

**Supplement Table T7.2: Statistical comparison of division angular spread atop anisotropic and isotropic substrates.** P-values for each comparison reveal a significant difference in division directionality between the anisotropic and isotropic substrates, however no difference between the two isotropic substrates. Significant differences following multiple comparison correction are highlighted in yellow. (W=wrinkled, NW=non-wrinkled, TCPS=tissue culture polystyrene).

| | W/NW | W/TCPS | NW/TCPS |
|---|---|---|---|
| p-value | <0.001 | <0.001 | 0.318 |

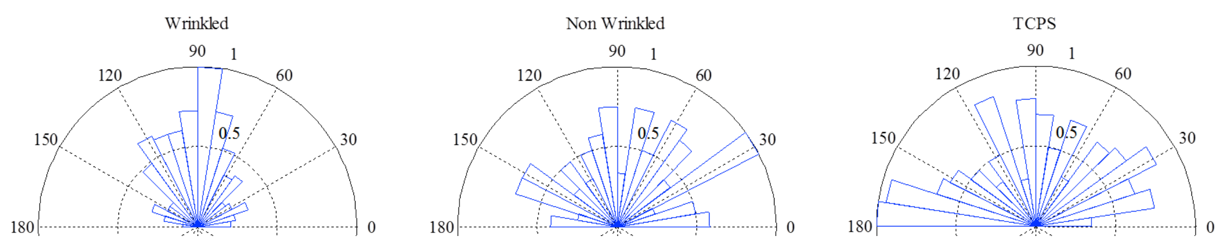


**Supplement Figure S7.1: Division angle atop anisotropic and isotropic substrates.** Representative angular histograms of the division angles atop wrinkled, non-wrinkled, and TCPS substrates reveal a narrow distribution of division angles for the wrinkled substrates, centered around 90° (parallel to the wrinkle direction), and broad distributions of division angles for both the non-wrinkled and TCPS substrates.

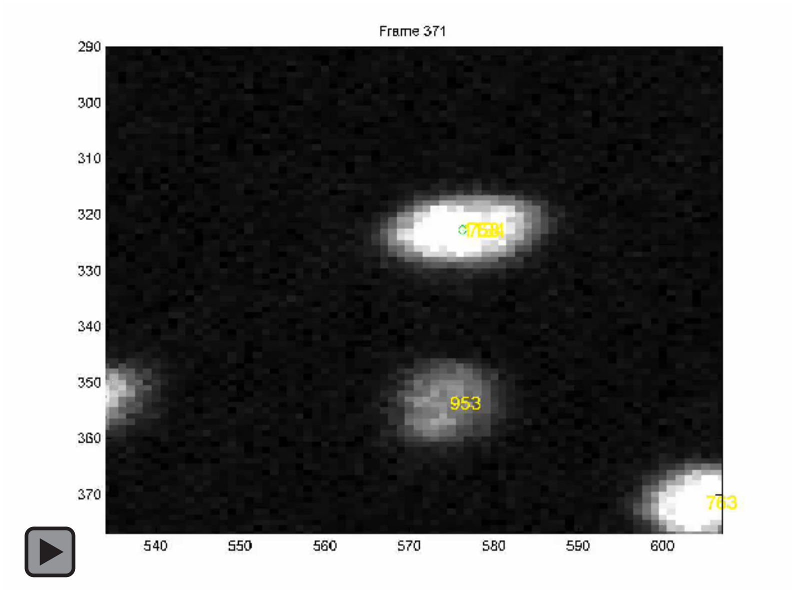


**Supplement Video V7.1: Example of correctly identified cell division.** The mother cell (initially tracked by the blue trail) splits into two daughter cells which are individually tracked by the ACT*IV*E system. Both daughter cells retain the track information of the mother cell after splitting apart.

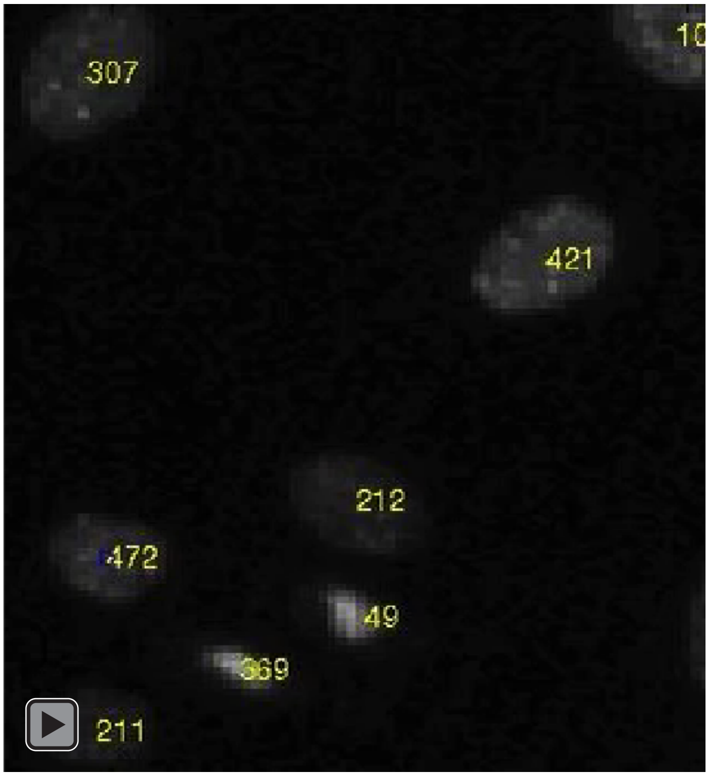


**Supplement Video V7.2: Example incorrect cell division identification due to complex merging event.** Complex interactions involving more than two cells can lead to the disappearance of one cell ID for several consecutive frames. Once that cell reappears, it is given a new ID and classified as a division.

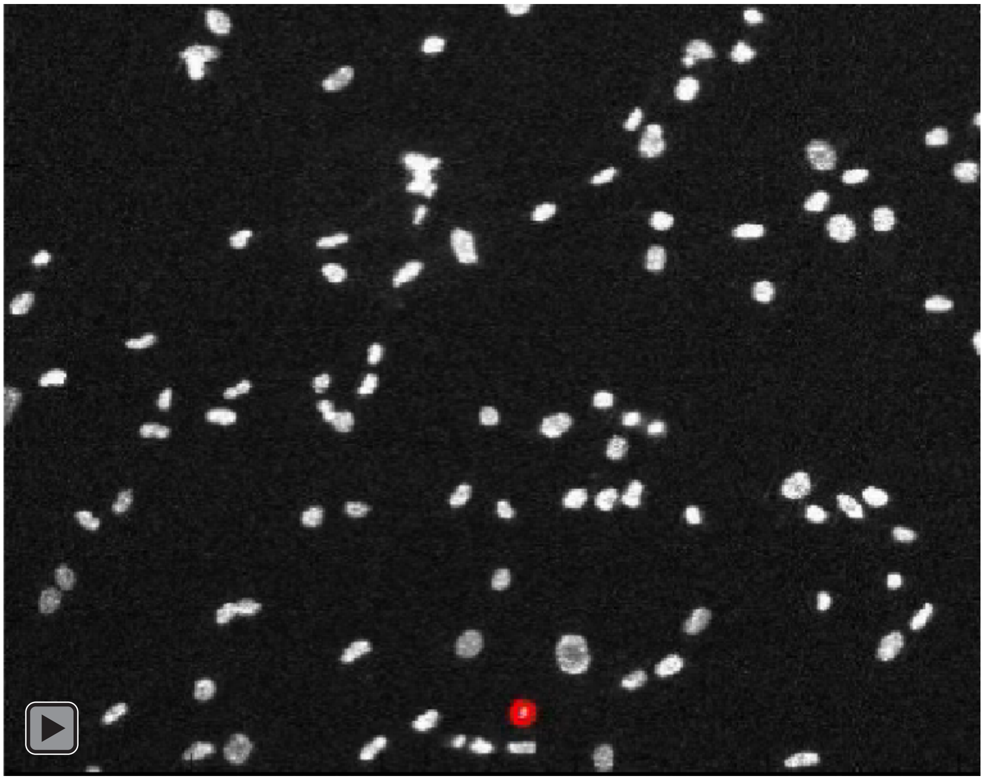

**Supplement Video V7.3: Example false negative investigation.** Cells tagged by ACT*IV*E as dividing cells are briefly labeled with red ellipses during the division process. An individual manually looks through the video for cell divisions that occur but that are not tagged with red ellipses. These missed cases are divisions that ACT*IV*E does not currently identify.

## Supplemental Information 8: Statistical Analysis

The following section summarizes the statistical comparisons conducted in this study.

### Supplemental Methods 8.1: Statistical Analyses

For comparisons between group and between substrates, nonparametric statistical analysis was performed because some of the combined samples deviated from the assumption of normality when subjected to a Shapiro-Wilks testing. Significance was determined at 95% confidence with Holms-Sidak correction for multiple comparisons. Supplement Tables T6.1 and T6.2 represent comparisons between groups for MSD, velocity auto-correlation, and cell track asphericity. Samples with p-values less than the adjusted critical p-value (according to Holm-Sidak correction) are highlighted in yellow. For comparisons within groups, parametric paired t-tests were conducted, with significance determined at 95% confidence. Supplement Table T6.3 summarizes the paired comparisons conducted in this study. Data used for the analysis is reported in Supplement Table T5.2 and T5.3.

**Supplement Table T8.1: P-values of MSD comparisons between substrates.** P-values are shown for each substrate comparison of wrinkled (W), non-wrinkled (NW), and tissue culture polystyrene (TCPS). Comparisons are shown for both the non-decomposed and decomposed MSD analyses. Highlighted values indicate significance following correction for multiple comparisons.

| | Non-decomposed MSD | | | Decomposed MSD | | | | | |
|---|---|---|---|---|---|---|---|---|---|
| Comparison | Short Timescale Slope | Long Timescale Slope | Mobility Intercept | X-Short Timescale Slope | X-Long Timescale Slope | X-Mobility Intercept | Y-Short Timescale Slope | Y-Long Timescale Slope | Y-Mobility Intercept |
| W/NW | 0.016 | 0.563 | 0.341 | 0.002 | 0.750 | 0.017 | 0.908 | 0.259 | 0.126 |
| W/TCPS | 0.118 | 0.019 | 0.403 | 0.008 | 0.056 | 0.665 | 0.325 | 0.885 | 0.019 |
| NW/TCPS | 0.583 | 0.049 | 0.100 | 0.583 | 0.040 | 0.061 | 0.506 | 0.174 | 0.371 |

**Supplement Table T8.2: P-values of velocity auto-correlation and asphericity comparisons between substrates.** P-values are shown for each substrate comparison (wrinkled = W, non-wrinkled = NW, and tissue culture polystyrene = TCPS). Comparisons are shown for both velocity auto-correlation decay constants and track asphericities. Highlighted values indicate significance following correction for multiple comparisons.

| | | Velocity Auto-correlation | | Asphericity |
|---|---|---|---|---|
| | Comparison | X-Time Constant | Y-Time Constant | Track Asphericity |
| Substrate | W/NW | 0.157 | 0.010 | 0.0002 |
| | W/TCPS | 0.000 | 0.119 | 0.0000 |
| | NW/TCPS | 0.001 | 0.126 | 0.0009 |

**Supplement Table T8.3: P-values of paired comparisons within substrates.** P-values are shown for each paired comparison, determining directionality differences within each substrate.. Comparisons are shown for both the non-decomposed and decomposed MSD analyses and the velocity auto-correlation analysis (VAC). Highlighted values indicate significance following correction for multiple comparisons.

| | | MSD | Decomposed MSD | | | VAC |
|---|---|---|---|---|---|---|
| | Group | Slope (Short - Long) | X Slope (Short - Long) | Y Slope (Short - Long) | Mobility Intercept (X-Y) | Time Constant (x-y) |
| Substrate | Wrinkle | 0.000 | 0.000 | 0.000 | 0.000 | 0.000 |
| | Non-wrinkle | 0.003 | 0.008 | 0.001 | 0.253 | 0.032 |
| | TCPS | 0.000 | 0.001 | 0.000 | 0.775 | 0.162 |

## References


1. Gao YX, Kilfoil ML. Accurate detection and complete tracking of large populations of features in three dimensions. Optics Express. 2009 Mar;17(6):4685-704.
2. Idema T. A new way of tracking motion, shape, and divisions. European Biophysics Journal. 2013:1-8.
3. Fitzgibbon A, Pilu M, Fisher RB. Direct least square fitting of ellipses. IEEE Transactions on Pattern Analysis and Machine Intelligence. 1999;21(5):476-80.
4. Henkes S, Fily Y, Marchetti MC. Active jamming: Self-propelled soft particles at high density. Physical Review E. 2011;84(4):040301.
5. Meijering E, Dzyubachyk O, Smal I. Methods for cell and particle tracking. Imaging and Spectroscopic Analysis of Living Cells: Optical and Spectroscopic Techniques. 2012;504:183-200. (DOI 10.1016/13978-0-12-3918574.00009-4).
6. Yang P, Baker RM, Henderson JH, Mather PT. In vitro wrinkle formation via shape memory dynamically aligns adherent cells. Soft Matter. 2013;9(18):4705-14.
7. Davidson P, Bigerelle M, Bounichane B, Giazzon M, Anselme K. Definition of a simple statistical parameter for the quantification of orientation in two dimensions: Application to cells on grooves of nanometric depths. Acta biomaterialia. 2010;6(7):2590-8.